Influence of gas hydrate morphology on the seismic velocities of sands

Jeffrey A. Priest,[1] Emily V. L. Rees,[1] and Christopher R. I. Clayton[1]

Received 31 December 2008; revised 30 June 2009; accepted 21 September 2009; published 26 November 2009.

[1] This paper reports the results of a series of resonant column tests on specimens where gas hydrate has been formed in sands using an ''excess water'' technique. In these specimens the amount of hydrate formed is restricted by the amount of gas in the specimen and with an excess of water being present in the pore space. Results of resonant column tests carried out to determine compressional and shear wave velocities suggest that gas hydrate formed in this way are frame supporting. In contrast, the behavior observed in sands where the hydrate is formed from finite water where the remaining pore space is saturated with methane gas, termed in this paper the ''excess gas'' method, exhibits a cementing behavior, while tetrahydrofuran-hydrate sands or where the hydrate is formed from dissolved methane within the pore water, exhibit a pore-filling behavior for hydrate saturations less than 40%. For sands where the hydrate is formed using the excess water method, much larger volumes of hydrate are required before a significant increase in shear wave velocity occurs, although increases in compressional wave velocity are seen at lower hydrate contents. These results suggest that hydrate interaction with the sediment is strongly dependent on morphology, and that natural hydrate may exhibit contrasting seismic signatures depending upon the geological environment in which it forms.

Citation: Priest, J. A., E. V. L. Rees, and C. R. I. Clayton (2009), Influence of gas hydrate morphology on the seismic velocities of sands, *J. Geophys. Res.*, *114*, B11205, doi:10.1029/2009JB006284.

1. Introduction

[2] The importance of gas hydrate either as an energy resource [*Collett and Ladd*, 2000; *Kerr*, 2004; *Ruppel*, 2007] as a driver for global climate change [*Kvenvolden*, 1993; *Haq*, 1998] or as a contributing factor in large submarine landslides [*Meinert et al.*, 1998; *Sultan et al.*, 2004; *Nixon and Grozic*, 2007], can only be fully assessed by accurately mapping the occurrence and concentration of hydrate within sediments and quantifying the effect that hydrates have on sediment properties. Natural gas hydrates are predominantly made from methane gas and water. Due to the temperature and pressure conditions that are required for their formation and stability [*Kvenvolden and Lorenson*, 2001], they are found in deep marine and subpermafrost sediments. Remote sensing techniques, measuring compressional wave velocity, V_p, and shear wave velocity, V_s, have been predominantly employed to obtain seismic data on these sediments [*Hyndman and Spence*, 1992; *Paull et al.*, 1996; *Collett et al.*, 1999; *Tréhu et al.*, 2003; *Expedition 311 Scientists*, 2005]. Various models have been hypothesized to correlate hydrate saturation to changes in the seismic velocities of the sediment [*Korenaga et al.*, 1997; *Helgerud et al.*, 1999; *Ecker et al.*, 2000; *Chand et al.*, 2004, 2006; *Lee and Waite*, 2008].

[3] The changes in seismic velocities are dependent on how hydrate interacts with the sediment, for example whether hydrate cements the sediment frame, fills the sediment pores without interacting with the sediment frame, or interacts with the sediment frame. Measurements of wave velocities of gas hydrate-bearing sediments are required to validate the model assumptions. However, due to the stability requirements for gas hydrate, obtaining intact hydrate sediment samples for detailed characterization has historically been very difficult, although recent success with pressure coring techniques have made this achievable [*Schultheiss et al.*, 2006, 2008]: unfortunately, current measurements techniques developed for these samples only provide limited characterization, and do not allow in situ stress conditions to be applied [*Yun et al.*, 2006].

[4] Because of these difficulties, research has focused on creating artificially synthesized gas hydrates within sediments in the laboratory. However, due to hydrate stability conditions, coupled with the low solubility of methane in water, the formation of homogeneously distributed methane gas hydrate in water-saturated sediments is challenging [*Stoll and Bryan*, 1979; *Winters et al.*, 2000]. There has been limited success in forming hydrate from gases in the dissolved phase [*Buffett and Zatespina*, 2000; *Spangenberg et al.*, 2005, 2008]. In these instances the formation times have been very long, and associated with a lack of control of the distribution of hydrate within the sediment, especially at low saturation values. Acoustic wave velocities for sediments with hydrate grown from dissolved gas suggest that the hydrate behaves as a frame-building component above 40% hydrate saturation, and pore-filling below [*Spangenberg et al.*, 2005, 2008].

[1]School of Civil Engineering, University of Southampton, Southampton, UK.

0148-0227/09/2009JB006284$09.00

[5] To overcome the limitation with methane solubility and lack of knowledge of hydrate location, laboratory studies have been conducted by forming hydrate from the free gas phase. Two different techniques have been utilized, which are herein referred to as the "excess gas" method and the "excess water" method. In the excess gas method a known volume of water is mixed with the sand prior to hydrate formation, with hydrate content being restricted by the amount of added water: the remaining pore space is filled with the hydrate-forming gas. This technique causes preferential growth of hydrate at grain contacts, which acts as a cement, producing a large increase in sediment strength and wave velocities even when small volumes of hydrate, of the order of 3–5%, are present [*Stoll and Bryan*, 1979; *Waite et al.*, 2004; *Ebinuma et al.*, 2005; *Priest et al.*, 2005]. In the excess water method, a known volume of gas is injected into the specimen, with water subsequently being injected until a target pore pressure within the specimen is achieved prior to hydrate formation. Hydrate content is restricted by the amount of gas that is added. *Yang et al.* [2008], using a similar technique measured wave velocity on specimens of sand, and sand/clay mixtures, with hydrate saturation varying from 24.6% to 34.3% (as calculated from the volume of gas injected). No measurements were obtained from nonhydrate-bearing sediments and so no comparison could be made as to the influence of the gas hydrate; although qualitatively the wave velocity for the sand specimen at 24.6% hydrate saturation was much lower than that observed for the same hydrate saturation using the excess gas method.

[6] An alternative approach has been to use tetrahydrofuran (THF) as an analog for methane as the hydrate former. The advantages of THF as a hydrate former are that it is miscible in water and the stability conditions are such that less specialist laboratory equipment is required. Results from tests using THF [*Kunerth et al.*, 2001; *Yun et al.*, 2005, 2007] suggest that THF has little effect on sediment strength or wave velocities until the hydrate volume is >40%, thereby suggesting a pore filling behavior. However, differences do exist between THF hydrate and methane hydrate. THF hydrate forms a type II structure rather than type I which is predominantly formed by methane [*Sloan*, 1998]. In addition, hydrate formation from solutions which do not have the ideal stoichiometric water/THF molar ratio of 17:1 may grow at preferential location points [*Zhang et al.*, 2001]. A detailed study by *Lee et al.* [2007] suggested that the differences between THF and methane as hydrate formers were minor compared to the effects of formation history within laboratory specimens and the pore scale distribution of hydrate within them.

[7] From the research highlighted above it can be seen that a variety of different mechanisms has been suggested for the interaction of hydrate with the sediment frame, depending on the formation process adopted. This paper adds to current knowledge by reporting on the seismic wave velocities measured in sand specimens containing methane gas hydrate formed using the excess water method and compares the results with that from specimens formed using the excess gas method. It is assumed that at the end of hydrate formation all free gas has been consumed and the specimen becomes saturated with water in the pore space: this may resemble typical gas hydrate-bearing environments.

2. Methodology

[8] This section describes the equipment used for our tests, the methods used for sand specimen preparation and methane hydrate formation, and the method of calculating the resulting proportion of pore space occupied by hydrate.

2.1. Equipment

[9] Specimens of single-size Leighton Buzzard sand containing known volumes of methane gas hydrate were tested in the gas hydrate resonant column (GHRC). The GHRC was developed by the authors [*Clayton et al.*, 2005; *Priest et al.*, 2005] to form methane gas hydrates within laboratory specimens under controlled temperature and pressure conditions. The GHRC allows a maximum confining pressure of 25 MPa with independent control of pore pressure. Temperatures can be controlled to 0.1°C from −20°C to +50°C.

[10] The resonant column apparatus (Figure 1) utilizes the theory of vibration of a linearly viscoelastic cylindrical rod to quantify the wave velocities [*Richart et al.*, 1970; *Drnevich et al.*, 1978]. The wave type generated within the specimen is dependent on the mode of vibration applied to the specimen. In the GHRC both torsional and flexural vibration [*Cascante et al.*, 1998] can be applied from which V_s and longitudinal flexural velocity (V_{lf}) can be calculated respectively. During a resonance test, a sinusoidal voltage is applied to the drive coils to induce a torsional or flexural oscillatory motion in the drive mechanism attached to the top of the specimen through the interaction of the attached magnets and the electromagnetic field generated by the coils. During a frequency sweep, the motion of the drive mechanism and the attached accelerometer produces an electrical output proportional to the induced acceleration. The resonant frequency of the specimen and drive mechanism corresponds to a peak in amplitude from the accelerometer, from which the wave velocity can be calculated. A detailed discussion of the resonant column test method and the data reduction techniques are given elsewhere [*Clayton et al.*, 2009].

2.2. Sample Preparation and Hydrate Formation

[11] The specimens were prepared using Fraction E Leighton Buzzard sand supplied by the David Ball Group, Cambridge, UK. This is a uniform fine sand, with 85% mean particle diameter between 90 and 150 μm by weight. Its grain density (specific gravity) is 2.65. Its minimum and maximum dry densities [*Rad and Tumay*, 1987; *Cresswell et al.*, 1999] are found to be 1331 kg/m^3 and 1624 kg/m^3 respectively. Minimum and maximum voids ratios calculated from the above dry densities are 0.633 and 0.993 respectively.

[12] Each specimen was prepared by tamping air-dried sand in 8–10 equal layers within a sample mold to form a dense, 70 mm diameter by 140 mm long, solid cylindrical specimen. Table 1 shows the actual dimensions, densities and initial porosities of the specimens tested along with the subsequent hydrate content. Specimens were sealed within a butyl rubber membrane (to minimize subsequent

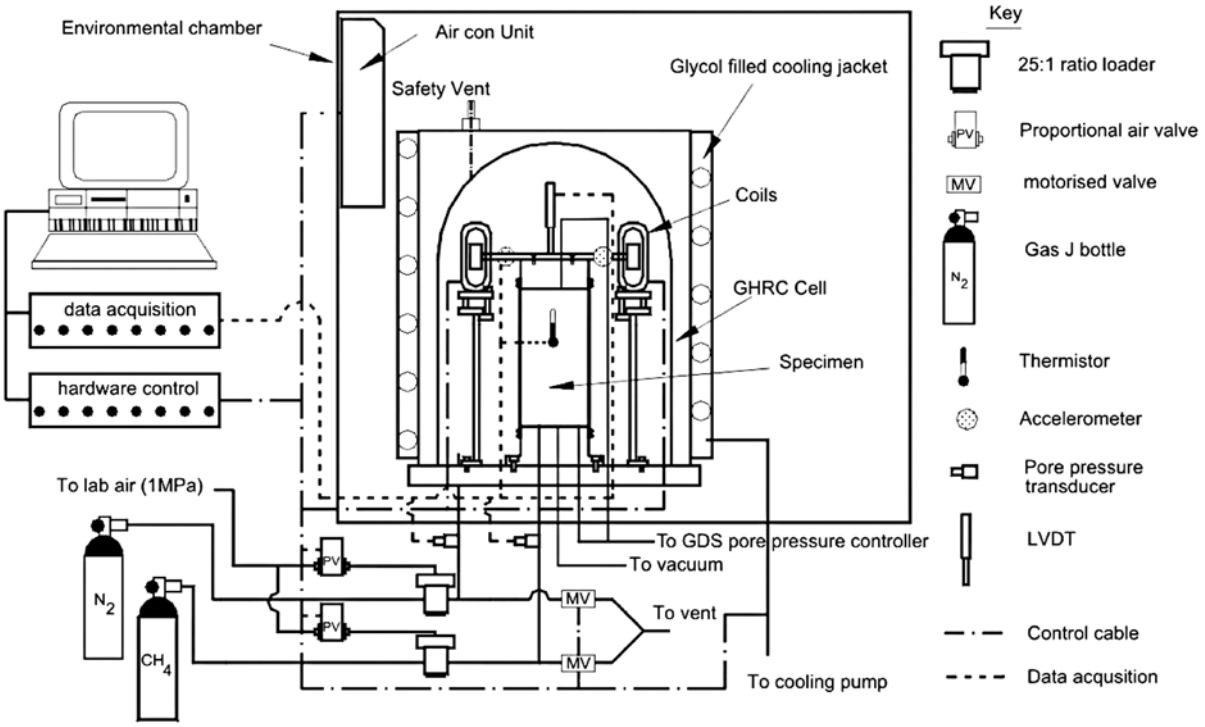

Figure 1. Schematic of resonant column apparatus with pressure and temperature control system and data acquisition system.

gas migration) to which thermistors were attached to the outside at mid height on opposite sides of the specimen to measure changes in temperature. A linear variable differential transformer (LVDT) displacement transducer was used to monitor the change in height of the specimen. After forming the specimens 60 kPa suction was applied to the specimen from a vacuum pump through the back pressure line and the resonant column drive system attached. The cell top was then fitted. A cell pressure was slowly applied while simultaneously releasing the vacuum, in order to provide a starting effective stress level (at point A in Figure 2) of 250 kPa under atmospheric back pressure and at room temperature. Then, methane gas was slowly injected into the pore space until a predetermined methane pressure was reached. This initial gas pressure was based on the amount of gas hydrate required in the pore space. The details of this calculation are described later. The cell and the pore pressure were simultaneously raised, so as to maintain an effective stress of 250 kPa±50 kPa. Once a predetermined pressure was reached, the methane gas supply was locked off. De-aired water was then injected into the specimen via the base pedestal and top cap until a predetermined water pressure was reached (point B in Figure 2), again while maintaining a 250 kPa ± 50 kPa effective stress.

[13] The cell temperature was lowered to 5°C (point C in Figure 2), thereby causing the pressure-temperature conditions within the specimen to cross the hydrate phase boundary, and initiate hydrate formation. During this process back pressure was kept constant while water was injected into the specimen, as the methane was consumed in the formation of hydrate. The specimen was kept in the hydrate stability field at 5°C for up to 7 days to allow complete hydrate formation. Full conversion of free gas to hydrate was deemed to have occurred once the measured resonant frequency of the specimen became constant (i.e., no further stiffening of the specimen due to hydrate could be detected) and no more water was required to maintain a

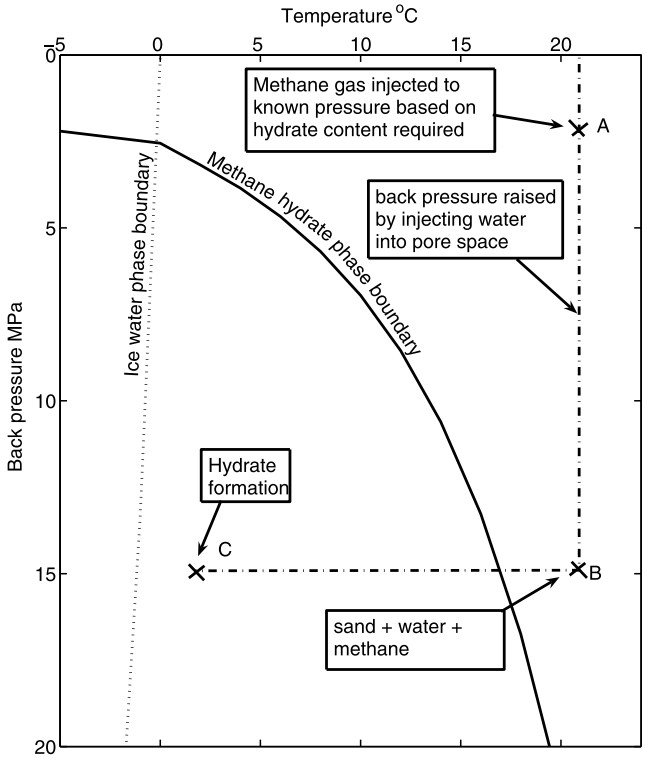

Figure 2. Pressure and temperature history during hydrate formation.

Table 1. Specimen Dimensions, Dry Densities, Initial Porosity, and Calculated Hydrate Pore Saturation

Specimen	Specimen Diameter (mm)	Specimen Height (mm)	Dry density (kg/m^3)	Initial Porosity	Hydrate Pore Saturation (%)
H0	70.5	140.2	1535.3	0.421	0
H10	70.4	142.6	1594.7	0.398	8.2
H15	70.2	144.6	1590.0	0.400	13.3
H20	70.2	141.5	1588.8	0.400	18.6
H30	70.3	142.4	1596.5	0.398	31.2
H40	70.5	142.8	1598.9	0.397	41.1

constant pore pressure. At this point resonant column measurements were started.

2.3. Calculations for Gas Hydrate Volume

[14] Using the excess water method, methane hydrate formed from free gas within the pore space. Hydrate volume was calculated from the number of moles of gas initially injected into the specimen, assuming 100% cage occupancy of both large and small cages of the structure 1 (SI) hydrate crystal. For laboratory synthesized hydrate this is thought to introduce less than 1% error [*Huo et al.*, 2003]. In these tests, where there is an abundant supply of water, one mole of methane gas will produce one mole of hydrate. The number of moles of methane gas, n, required for a given hydrate pore saturation (H_c (%)) can be calculated from

$$\frac{V_v H_c \rho_H}{100 M_H} = n \tag{1}$$

where V_v is the volume of the pore space (m^3), ρ_H is the density of hydrate (910 kg/m^3 [*Sloan*, 1998]), and M_H is the molar mass of methane hydrate (0.11963 kg/mol [*Sloan*, 1998]). As the volume of pore space, V_v, is defined by dimensions of the specimen and the volume of sand added, the number of moles of methane gas injected into the pore space can be calculated from the measured pore pressure within the specimen through the Peng-Robinson equation of state [*Peng and Robinson*, 1976];

$$p = \frac{RT}{V_m - b} - \frac{a\alpha}{V_m^2 + 2bV_m - b^2} \tag{2}$$

where

$$a = \frac{0.45724 R^2 T_c^2}{p_c} \tag{3}$$

$$b = \frac{0.07780 R T_c}{p_c} \tag{4}$$

$$\alpha = \left(1 + \left(0.37464 + 1.54226\omega - 0.26992\omega^2\right)\left(1 - T_r^{0.5}\right)\right)^2 \tag{5}$$

$$T_r = \frac{T}{T_c} \tag{6}$$

$$V_m = \frac{V_v}{n} \tag{7}$$

[15] R is the ideal gas constant (8.314472 $\times$ 10^{-6} m^3.MPa.K^{-1}.mol^{-1})), T_c is temperature of methane gas at the critical point (190.6 K (National Institute of Standards and Technology (NIST), NIST Chemistry WebBook, 2005, available at http://webbook.nist.gov/chemistry)), P_c is pressure of methane gas at the critical point, (4.656 MPa (NIST, 2005)), ω is the acentric factor for methane gas (0.0108 [*Chapoy et al.*, 2004]).

[16] Some of the free methane gas dissolved in the pore water as the back pressure was raised. Using the solubility values given by *Handa* [1990] and taking into account the volume of pore water in the specimen and water pressure system (water in lines and digital pressure controller), the number of dissolved moles of methane was calculated for each specimen. This value was added to the calculated number of moles obtained using equation (1) with the combined value being used in equation (2) to calculate the initial gas pressure required for each specimen.

3. Results and Discussion

[17] In total, five specimens with different volumes of hydrate pore saturation were formed using the excess water method described above (Table 1). Target hydrate pore saturations were 10, 15, 20, 30 and 40%. Specimen permeability reduced during hydrate formation such that above 40% hydrate pore saturation the injection of water into specimens was severely restricted and effective stress control could not be maintained.

3.1. Hydrate Formation

[18] Table 2 lists the starting pressure applied to each specimen based on the calculated hydrate volume required. Figure 3 shows the change in water intake and temperature with time for specimen H30 (target hydrate content of 30%) during the hydrate formation stage. At position A the pore volume of the specimen is filled with methane gas to the initial target pressure as given in Table 2, Stage A to B is due to the injection of water into the specimen up to the target back pressure of 18 MPa (highlighted in section 2.2). The temporary rise in measured specimen temperature that occurred during this stage (A to B) was due to the adiabatic temperature increase of the nitrogen cell gas as the cell pressure was raised to maintain the 250 kPa ± 50 kPa effective stress. At position B, the specimen was held overnight at constant temperature and pressure to allow system equilibration, and insure no leaks were present. Gas dissolving into solution was offset by small increases in water intake. At position C, the cell temperature was lowered to 2.5°C over an eight hour period and subsequently maintained at this temperature until hydrate formation ceased (position D).

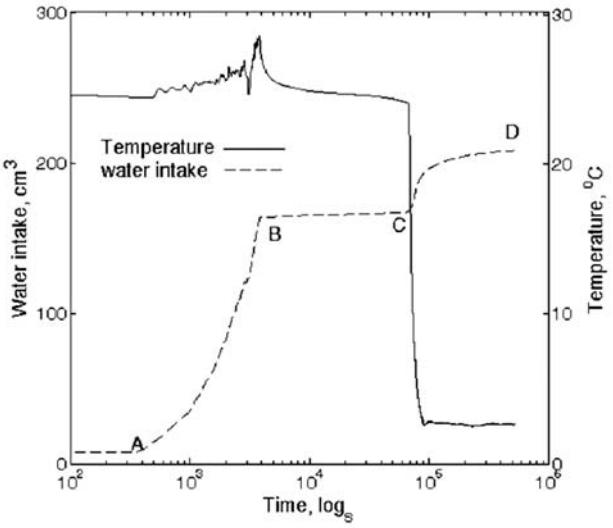

Figure 3. Water intake with time during pressure ramp and subsequent hydrate formation stage for specimen H30 (30% hydrate target). Also shown is the specimen temperature with time.

[19] Figure 4 shows the change in water intake with specimen temperature during the hydrate formation stage (position C to D in Figure 3). At point C, where the specimen temperature starts to decrease, a corresponding increase in water intake occurs with a linear rise until a specimen temperature of about 15°C is reached. This increase is expected due to the reduction in methane gas pressure as a result of the change in temperature (equation (2)). From about 15°C to ~7.8°C, the rate of water intake increased slightly. This increase in rate of water intake is thought to coincide with the onset of hydrate nucleation within the pore space of the specimen. The target back pressure chosen during this test (18 MPa) would suggest that hydrate formation, for bulk hydrate, should commence at around 18.6°C [*Sloan*, 1998]. The discrepancy between the theoretical start of hydrate formation and that recorded here is more likely to have been caused by the internal specimen temperature lagging the external cell temperature, rather than small pore sizes reducing the theoretical temperature for hydrate stability [*Clennell et al.*, 1999; *Anderson and Tohidi*, 2005]. At ~7.8°C the water intake increases rapidly as mass hydrate formation starts to occur. Beyond position D no further water input is required to maintain the back pressure, suggesting that hydrate formation is complete.

[20] The total volume of water injected into the specimen during the test was 208.56 cm^3. Given the total volume of the pore space for this specimen (221.3 cm^3) and the expected volume of hydrate (69.72 cm^3, calculated from equation (1)), the total volume of water required to saturate the specimen (including hydrate water (assuming a 5.75:1 molar ratio of water/CH_4) and free water) would equate to 206.97 cm^3 a volume error of about 1%.

[21] Table 2 shows the volume of water that was taken up by each of the specimens during hydrate formation. Typically, the discrepancy between the calculated water volume required to saturate the specimen after hydrate formation and that actually taken up for each specimen is less than 1%, although specimen H20 was somewhat higher (2.86%). More water was taken up by the specimens than initially calculated. Even with uncertainties in sample dimensions and void ratio, the small errors between calculated and measured water volumes strongly suggest that after hydrate formation each specimen was fully saturated with little or no free gas within the pore space.

[22] The distribution of hydrate within the specimen is dependent on where the gas is located at formation. In these tests the sand was initially dry, with methane gas in the pore space. It was assumed that water injection would not globally displace the methane gas (compress it into the top or the bottom of the specimen) but would form gas bubbles within each pore throat, the bubble size being dependent on the total volume of water injected and the initial gas pressure (the water was injected through porous discs, which distributes the water over the whole diameter of the sample, in about 30 min).

[23] Under this assumption the gas hydrate will be uniformly distributed throughout the specimen. To investigate this, water contents were measured on depressurized samples. Depressurization occurred by slowly reducing cell and pore pressures while allowing drainage through the base (only). Once atmospheric pressure was reached the specimens were removed and subsectioned. Table 3 shows water content results on horizontal subsections for four specimens. Except for the top section, the water content for each of the specimens was reasonably consistent. The lower water contents in the top sections of the specimens may result from higher gas content at the top of each specimen, or gravitational drainage from the base of the specimen during depressurization.

3.2. Shear Wave and Flexural Velocity

[24] In the resonant column test V_s and V_{lf} can be directly obtained from the torsional and flexural vibration of the specimens, respectively. Seismic velocity measurements for

Table 2. Calculated Water Volume to Create 100% Conversion of Gas to Hydrate and Measured Volume of Water Taken Up by Each Specimen During Hydrate Formation

Specimen	Gas Pore Pressure (kPa)	Calculated Water Volume (mL)	Measured Water Volume (mL)	Volume Error Between Calculated and Measured Values (mL)	Error (%)
H10	2410	217.27	219.07	1.8	0.83
H15	3236	216.70	217.51	0.81	0.37
H20	4028	210.48	216.50	6.02	2.86
H30	6013	206.97	208.56	1.59	0.77
H40	7044	203.14	203.47	0.33	0.16

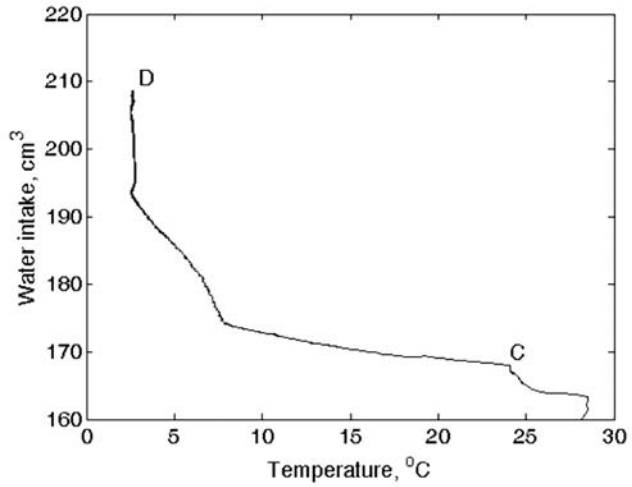

Figure 4. Plot of water intake with specimen temperature for specimen H30 during the hydrate formation stage C–D as highlighted in Figure 3.

the five hydrate-bearing sand specimens formed using the excess water method, and one water-saturated sand specimen with no hydrate are presented in Table 4 for resonant column tests carried out under an effective confining pressure of 500 kPa. The influence of hydrate pore saturation on the seismic velocities (V_s and V_{lf}) of these sand specimens subject to isotropic loading and unloading is shown in Figure 5. Also shown is the response of a sand specimen with 10% hydrate pore saturation formed using the excess gas method [*Priest et al.*, 2005].

[25] For the hydrate-bearing sand specimens formed using the excess water method no appreciable change in V_s and V_{lf} is apparent for specimens with up to 20% hydrate pore saturations. Above 20% both V_s and V_{lf} increase with increasing hydrate pore saturation. Increases of 34% and 22% for V_s and V_{lf}, respectively, are observed for specimen H40 compared to specimen H0. In contrast, for the specimen with 10% hydrate saturation formed using the excess gas method, V_s and V_{lf} increased by about 207% and 254% as a result of adding hydrate. In addition, using the excess gas method, V_s and V_{lf} were almost independent of effective confining pressure (at 10% hydrate saturation) compared to the excess water method where the velocity response of all specimens was similar to that for the sand specimen with no hydrate in the pore space.

[26] For granular soils subjected to an isotropic effective stress, σ', it can be shown that V_s and V_{lf} can be related to σ' through a simple exponential relationship of the form

$$V = A\sigma'^{b}, \tag{8}$$

where A and b are constants [*Hardin and Black*, 1968; *Hardin and Drnevich*, 1972]; b represents both the nature of the contact stiffness and fabric change (porosity, number of contacts) as a function of isotropic confining stress [*Cascante et al.*, 1998]. The power exponents b_s and b_{lf}, obtained from V_s and V_{lf}, respectively, are shown in Figure 6. These exponent values are obtained by fitting equation (8) to the velocity/load response of the specimens shown in Figures 5a and 5b. Also plotted are b_s and b_{lf} obtained from specimens formed using the excess gas method. For the excess water specimens, addition of hydrate into the pore space causes no, or only minor, changes (for hydrate saturations above 20%) in both b_s and b_{lf} compared to the nonhydrated specimen, with the measured values being within the range expected for normal clean sands [*Hardin and Drnevich*, 1972; *Cascante et al.*, 1998]. The results suggest that hydrate formation using the excess water method does not alter, to any significance, the grain contact stiffness. Minor variations in b_s and b_{lf}, at higher hydrate saturation (where effective porosity reduces) may result from hydrate grains stabilizing grain contacts through increased buckling resistance to force chains [*Santamarina et al.*, 2001; *Makse et al.*, 2004], such that rotation of the contacts are frustrated thereby giving rise to an increase in wave velocity. This effect is similar to that which would result from reduction in porosity, or increase in confining pressure. In contrast the excess gas method leads to a rapid reduction in both b_s and b_{lf} to values of about 0.01–0.05 for hydrate pore saturation greater than ~3–5%, highlighting that wave velocity is independent of confining pressure due to the cementing effect of the gas hydrate [*Clayton et al.*, 2005]. This is similar to the results obtained for other cemented sands [*Chang et al.*, 1990; *Saxena et al.*, 1988].

3.3. Compressional Wave Velocity, V_p

[27] In offshore seismic surveys compressional wave (V_p) velocities are routinely used to infer the presence of hydrate [*Kvenvolden and Barnard*, 1983; *Hyndman and Spence*, 1992; *Dillon et al.*, 1994; *Korenaga et al.*, 1997]; therefore, it is important to examine the effects of hydrate formation on V_p. In the resonant column, flexural velocity, V_{lf}, obtained from flexural excitation of the specimen, can be used to calculate V_p.

[28] During flexural excitation the strain field has a linear distribution, varying from tension to compression across the horizontal specimen section [*Cascante et al.*, 1998]. At high flexural frequencies relative to the permeability of the test medium there is insufficient time for significant internal cross-specimen drainage, the resonant frequency in flexure will therefore be affected both by the increase in bulk modulus caused by the pore water and by the increase in density of the specimen. However, comparison between results for dry and saturated (hydrate-free) Leighton Buzzard E sand specimens show that the effect of saturation can be

Table 3. Water Content for Selected Specimens After Depressurization and Dissociation[a]

	Test Specimen			
Section	H10	H20	H30	H40
Top	12.2	11.1	10.5	8.4
	15.6	13.7	12.7	11.2
				11.0
	15.8	14.1	13.8	11.6
				12.2
	15.9	14.6	14.1	12.4
Bottom	15.6	14.4	13.1	11.6

[a]Water content in % by weight of dry sand. For specimens H10–H30 each specimen was divided into five equal sections, while for specimen H40, seven equally spaced sections were obtained.

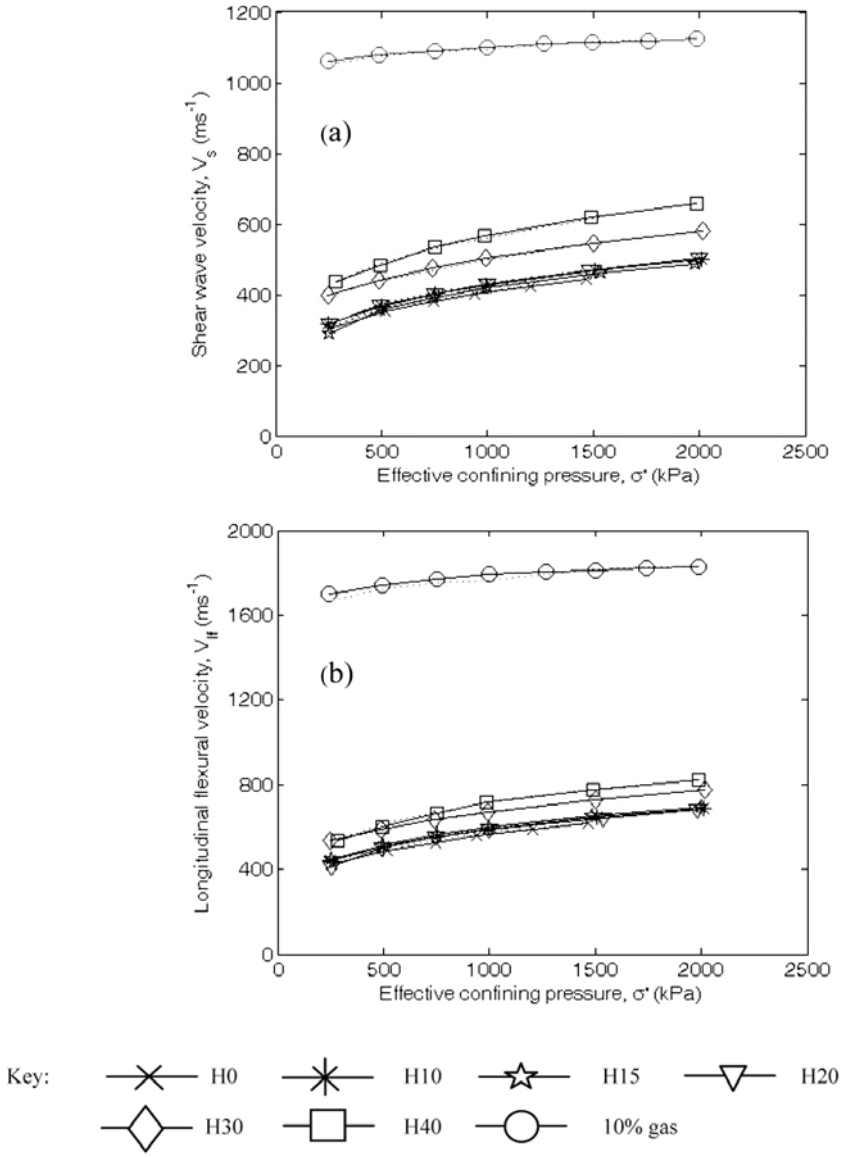

Figure 5. (a) Shear wave velocity (V_s) and (b) Longitudinal flexural wave velocity (V_{lf}) with effective confining pressure (σ') for excess water specimens listed in Table 1. Data are also included from *Priest et al.* [2005] for an excess gas specimen containing 10% hydrate.

predicted by taking into account the increase in specimen bulk density alone, thus showing that at these frequencies internal lateral drainage occurs. Therefore, to derive V_p using the measured V_{lf} values the stiffness of the pore water needs to be taken into account as suggested by *Gassmann* [1951].

[29] Figure 7 shows the calculated saturated V_p values for the excess water specimens highlighted in Table 1 along with the response of an excess gas specimen with 10% hydrate pore saturation. The results show that V_p is more susceptible to the influence of gas hydrate in the excess water specimens than both V_s and V_{lf} (from Figure 5), with the variation between individual specimens, especially at low hydrate pore saturation ($\leq$20%), being more distinguishable. In addition, the difference in V_p between specimen H40, which has 40% hydrate pore saturation, and the excess gas specimen that has 10% hydrate pore saturation, is much less than that observed for V_s and V_{lf}. This susceptibility is primarily attributable to the bulk modulus of the pore water dominating the computed V_p values.

[30] Figure 8 shows the comparison of V_p/V_s ratios for the excess water specimens and the excess gas specimens at a confining pressure of 500 kPa. For the excess water speci-

Table 4. Seismic Wave Velocities of Water-Saturated Hydrate-Bearing Sediments at an Effective Confining Pressure of 500 kPa

Specimen	V_s (m s^{-1})	V_{lf} (m s^{-1})	V_p (m s^{-1})
H0	347	491	1655
H10	359	507	1747
H15	364	514	1772
H20	353	502	1802
H30	434	589	1922
H40	470	600	2006

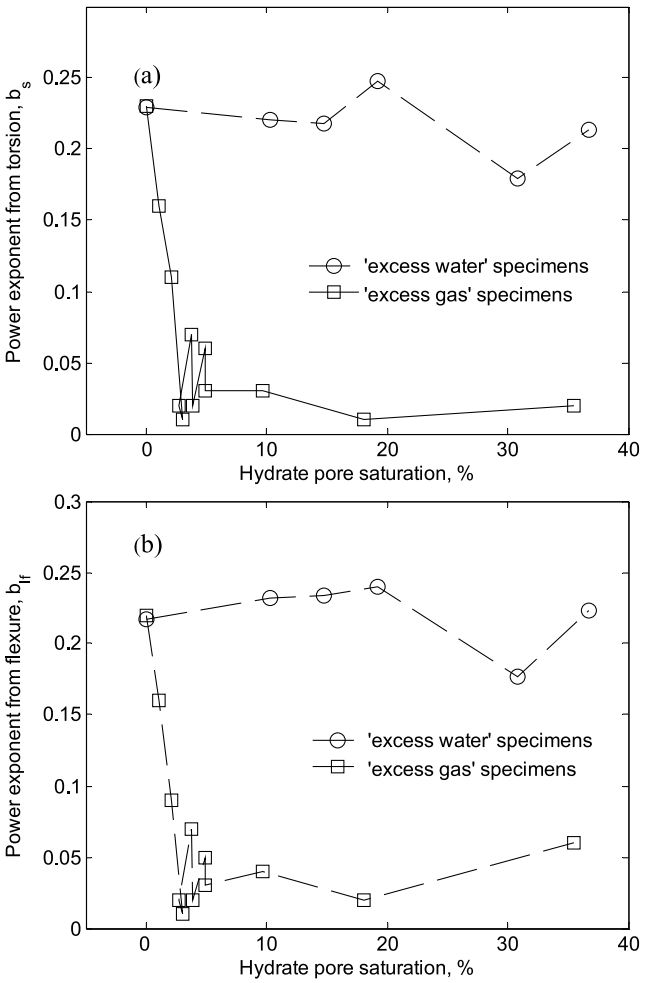

Figure 6. (a) Power exponent b_s from shear wave velocity and (b) power exponent b_{lf} from longitudinal velocity during isotropic loading for excess water specimens (open circles) and excess gas specimens (open squares) from *Priest et al.* [2005].

mens there are minor differences in the computed V_p/V_s ratio as the hydrate pore saturation increases, whereas for the excess gas specimens V_p/V_s ratios drop dramatically with increasing hydrate pore saturation. The calculated V_p/V_s ratios for the nonhydrated specimen and excess water specimens are comparable to values measured in the field at low confining pressures [*Hamilton*, 1971; *Hamilton*, 1979; *Prasad*, 2002; *Duffaut and Landrø*, 2007; *Zimmer et al.*, 2007]. The minor increase in the V_p/V_s ratio from specimens H0 to H20 result from the increase in V_p (Figure 7), without any corresponding increase in V_s (Figure 5a). For higher hydrate saturations (H30 and H40) the hydrate causes a larger increase in V_s (from that of the nonhydrate-bearing specimens) compared to V_p and so reducing the V_p/V_s ratios. For the excess gas specimens V_p becomes less dominated by the bulk modulus of the pore fluid and more by the increasing cementation of the sand grains. This leads to a large reduction in the velocity difference between V_p and V_s and therefore significant changes in V_p/V_s ratios occur, dropping from about 5 for the nonhydrate-bearing specimens to about 2 for when bonded by hydrates, values similar to those observed for consolidated rocks [*Castagna et al.*, 1985; *Wilkens et al.*, 1984; *Shillington et al.*, 2008].

[31] Also shown in Figure 8 is the influence of effective confining pressure on the V_p/V_s ratio for the excess water specimens. It can be seen that the response for all specimens is similar, with V_p/V_s reducing with increasing confining pressure. At higher confining pressures than used in these experiments it has been shown that V_p/V_s ratio for saturated soils reduces to a limiting value of 2 and becomes independent of confining pressure [*Domenico*, 1977; *Bachrach et al.*, 2000; *Makse et al.*, 2004; *Duffaut and Landrø*, 2007; *Zimmer et al.*, 2007; *Yang et al.*, 2008]. This value is similar to that obtained for the excess gas specimens where both V_p and V_s are independent of confining pressure.

[32] The results suggest that for naturally occurring hydrate-bearing sediments, where the hydrate formation is similar to the excess water method, the V_p/V_s ratio will be dependent on porosity, confining pressure and hydrate content and therefore quantification of hydrate pore saturation from either V_s, V_p or V_p/V_s ratios would be difficult without a detailed knowledge of the sediment properties and stress state.

3.4. Comparison of Laboratory-Derived Wave Velocities and Model Predictions

[33] As already noted a number of modeling approaches have been adopted to try and understand the influence of gas hydrate on the propagation of wave velocities in marine sediments. A key assumption that needs to be considered is how the hydrate interacts with the sediment, i.e., is it pore filling, frame building or cementing. In this paper the modeling approach of *Helgerud et al.* [1999] is adopted. This uses a modified Hashin-Shtrikman Hertz Mindlin theory proposed by *Dvorkin and Nur* [1996] to calculate the dry elastic moduli of the sediment frame and the subsequent saturated sediment moduli using Gassmann's equations [*Gassmann*, 1951]. If the hydrate is pore filling then this is accounted for by modifying the bulk modulus of the pore fluid to account for the addition of gas hydrate. In the cementation model the hydrate is assumed to grow at grain contacts, greatly increasing the stiffness of the sediment frame [*Dvorkin and Nur*, 1993]. The elastic properties used for the constituent mineral grains and the pore fluid within the modeling are given in Table 5.

[34] Figure 9 shows the saturated wave velocities for V_p and V_s as a function of hydrate pore saturation for all the excess water specimens at $\sigma' = 500$ kPa during isotropic loading, along with results from *Priest et al.* [2005] using the excess gas method. Also presented are the theoretical curves for V_p and V_s. In the modeling the effective confining pressure is arbitrarily chosen so that the derived wave velocity matches that obtained from the saturated nonhydrate-bearing sand specimen. From Figure 9 it can be seen that both V_p and V_s for the excess water specimens closely follow those for the frame supporting model. Although not shown, alternative theoretical models [*Lee and Collett*, 2005; *Lee and Waite*, 2008] also suggest a frame supporting behavior for the hydrate saturations tested. Results from *Yang et al.* [2008], using a similar hydrate saturation technique, also suggest a frame supporting behavior. In contrast, results for the excess gas specimens both for V_p and V_s cannot adequately be described by either the cemen-

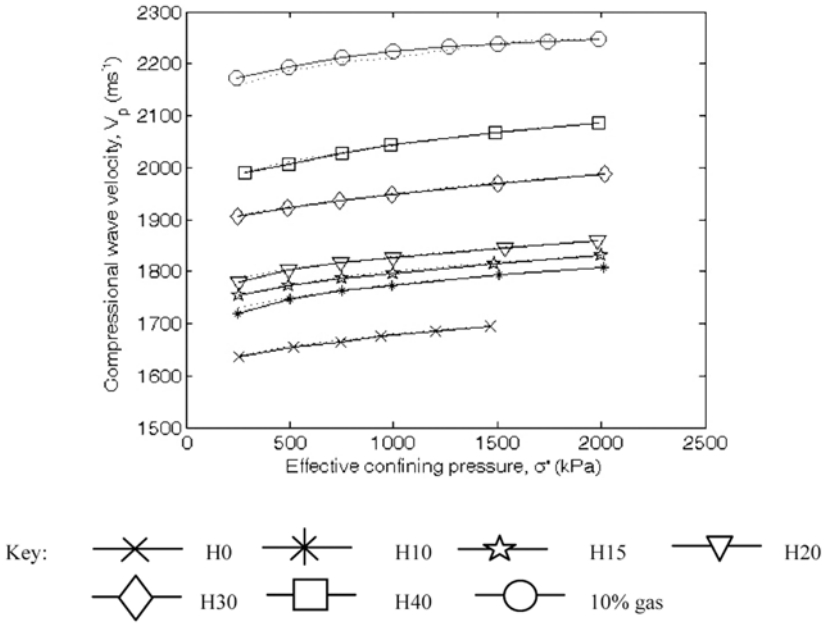

Figure 7. Compressional wave velocity with effective confining pressure (σ) for excess water specimens listed in Table 1. Also included are data for an excess gas specimen containing 10% hydrate.

tation model or frame supporting model and therefore these specimens may exhibit a combination of both cementing and frame supporting behavior [*Chand et al.*, 2006]. Results from other studies, using variations of the ''excess gas technique'' also show a cementing behavior [*Waite et al.*, 2004; *Winters et al.*, 2004].

[35] Figure 10 shows an interpretation of where the hydrate might reside given the different formation techniques adopted. In sands where hydrate is formed using the excess gas method and water is restricted to grain surfaces and contacts (through surface tension), hydrate forms at the grain contacts, leading to cementation of the sand grains at low hydrate concentrations. As hydrate saturation increases, the degree of cementation as a function of hydrate saturation reduces. In sand specimens formed using the excess water method the hydrate forms around the initial gas bubbles [*Tohidi et al.*, 2001], which reside in the pore space, such that individual hydrate grains may not be interconnected with each other. As hydrate saturations increase the hydrate grains start to interact with the sediment, helping restrict buckling of the ''force chains'' [*Makse et al.*, 2004] and increasing the number of particle contacts (coordination

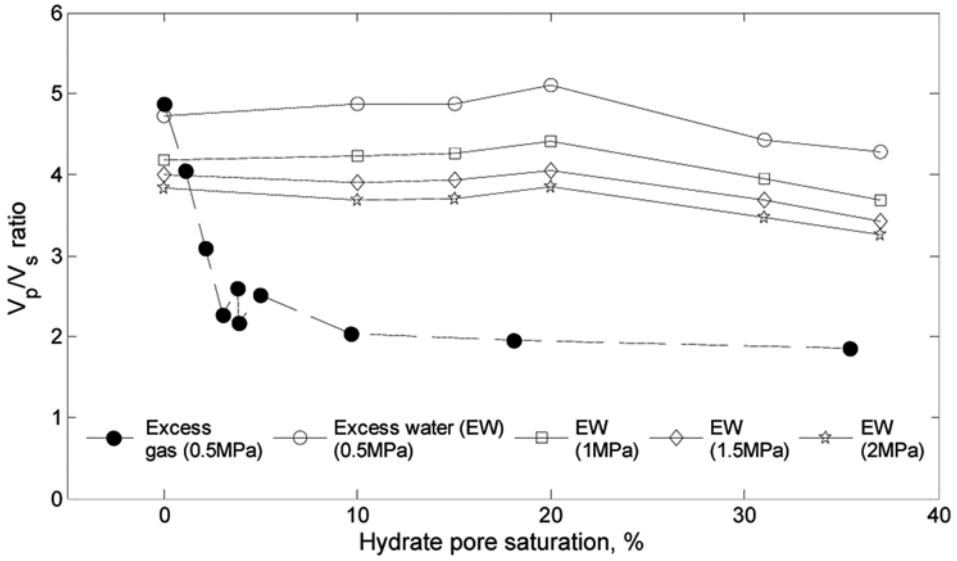

Figure 8. Comparison of computed V_p/V_s ratios for excess water (EW) specimens and excess gas specimens from *Priest et al.* [2005].

Table 5. Elastic Properties Used in Modeling Wave Speeds in Sediments as Presented in Figure 9

Parameter	Value
Shear modulus of sand grains[a] (GPa)	45
Bulk modulus of sand grains[a] (GPa)	36.6
Shear modulus of hydrate[b] (GPa)	7.9
Bulk modulus of hydrate[b] (GPa)	3.3
Bulk modulus of pore fluid[c] (GPa)	2.25

[a]*Carmichael* [1982].
[b]*Helgerud et al.* [1999].
[c]*Mavko et al.* [1998].

number), and the contact area. This will lead to frustration of particle rotation and more effective transmission of the shear wave through the specimen. At low hydrate saturations the bubble size may be small relative to the sand grain such that this effect is limited, but it can be expected to increase with hydrate saturation.

4. Conclusions

[36] A series of tests has been presented for specimens containing hydrate formed using an excess water technique that allowed for the controlled formation of disseminated gas hydrate, where the volume of gas hydrate formed in the specimen was quantified from the initial number of moles of gas in the specimen. The technique allows gas hydrate to form within the pore space between the sand grains, probably at gas bubble/water interfaces. This morphology is distinct from that produced previously used by the authors, using the excess gas method, where limited water concentrated methane hydrate forma-

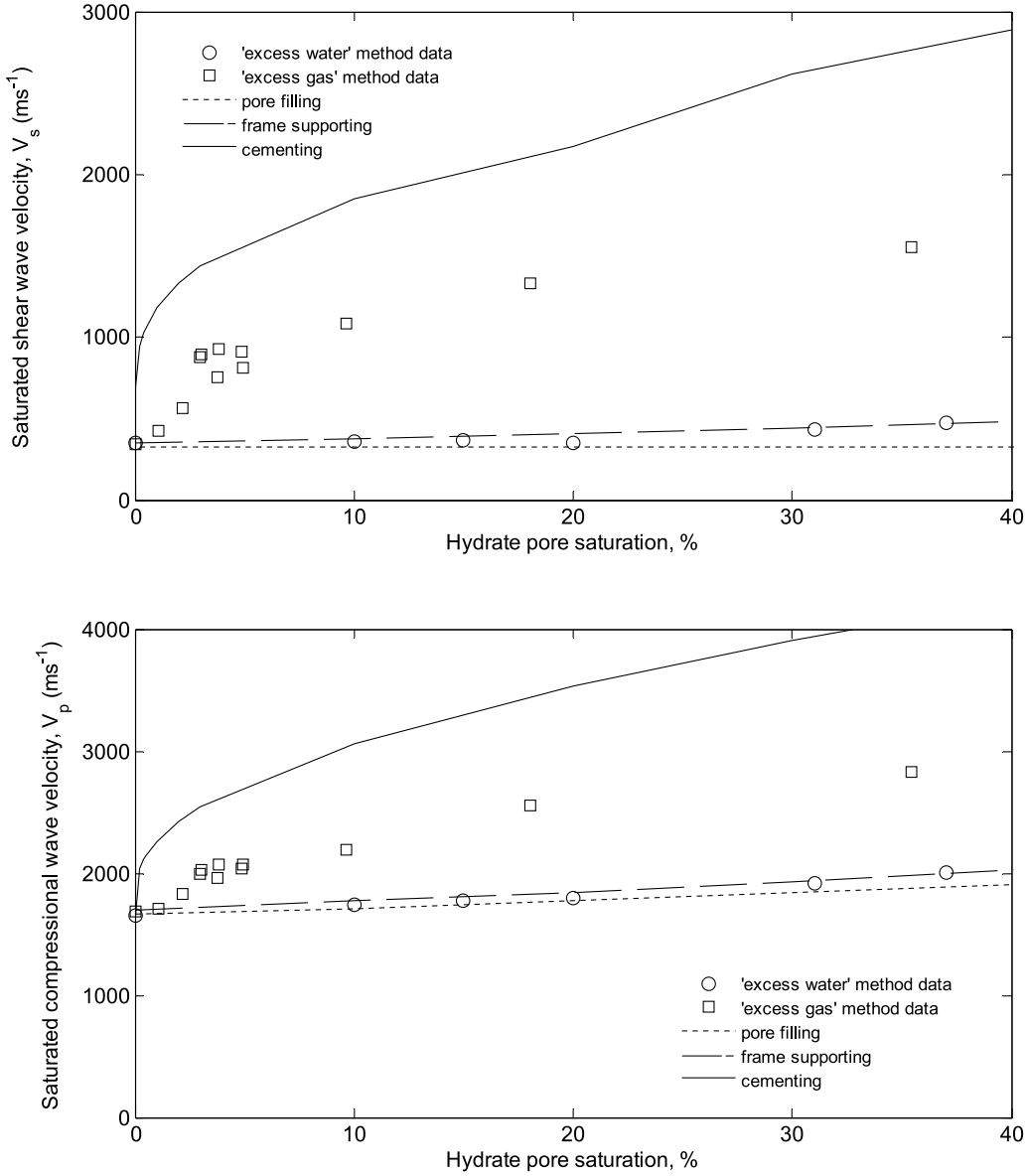

Figure 9. Variation in V_p and V_s with hydrate pore saturation for excess water specimens (open circles) and excess gas specimens from *Priest et al.* [2005] at a confining pressure of 500 kPa. Theoretical V_p and V_s values are also shown for pore-filling model (dotted line), frame supporting model (dashed line) and cementing model (solid line).

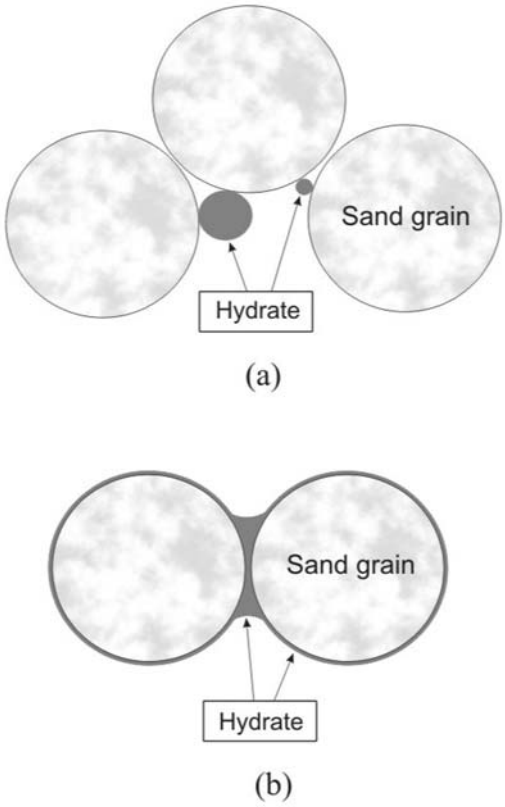

Figure 10. (a) Location of hydrate in the pore space formed using excess water method: Hydrate forms around gas bubbles. (b) Location of hydrate formed using excess gas method: hydrate forms where water collects at grain contacts.

tion at the grain contacts. Both morphologies may occur in nature.

[37] Velocity measurements, V_s and V_{lf}, obtained using a resonant column show that hydrate formed using the excess water method had no apparent effect on the measured velocities of a sand until hydrate saturation was greater than 20% of the pore space, in contrast the excess gas method led to a rapid increase in wave velocity. Measurements of the velocity-stress exponent b, for both shear and longitudinal flexural velocity, showed that excess water specimens had minor influence on b suggesting that no appreciable increase in grain contact stiffness occurs, although at higher saturations the hydrate may help stabilize grain contacts. In contrast the excess gas specimens reduce b to near zero, highlighting the stress independent behavior of these specimens. It was shown that V_p, which was indirectly computed in this study, was more susceptible to hydrate, and changes in V_p could be identified at hydrate saturations below 20%, which were not evident in either V_s or V_{lf} measurements.

[38] For the excess water hydrate-bearing specimens it was shown that the V_p/V_s ratio was only marginally affected by hydrate once the hydrate pore saturation was above 20%. The marginal change in V_p/V_s results from relatively larger changes in V_s than V_p, since V_p is dominated by the bulk modulus of the water. In contrast the excess gas hydrate-bearing specimens showed a drastic reduction in V_p/V_s to values of about 2, similar to that for consolidated rocks.

[39] Comparison of theoretical models for both V_p and V_s (where the hydrate is assumed to exhibit a pore-filling behavior, or a frame-supporting behavior, or a cementation behavior) with the measured V_p and V_s values suggest that for the excess water specimens the hydrate exhibits a frame supporting behavior, similar to that observed by *Yang et al.* [2008]. For the excess gas specimens the hydrate exhibits a cementing behavior, similar to that observed by others using similar techniques [*Stoll and Bryan*, 1979; *Waite et al.*, 2004; *Winters et al.*, 2004; *Ebinuma et al.*, 2005]. For hydrates formed out of solution [*Spangenberg et al.*, 2005, 2008], or using THF as the hydrate former [*Yun et al.*, 2005], a pore filling behavior is observed for hydrate saturations of less than 40%.

[40] Results from the laboratory studies conducted by the authors and comparison with other laboratory observations suggest that the influence of gas hydrate on the physical properties of sediments is strongly dependent on the morphology of the hydrate. As such, careful assessment of possible formation mechanisms must be considered when inferring hydrate contents from the changes in physical properties of natural in situ gas hydrate-bearing sediments.

[41] **Acknowledgments.** The work described in this paper was funded by the UK Engineering and Physical Sciences Research Council (grant EP/D035996/1). The authors would like to thank the JGR Associate Editor and the reviewers for their constructive comments and suggestions during the review process.

References

Anderson, R., and B. Tohidi (2005), Capillary pressure controlled methane hydrate growth and dissociation hysteresis in narrow interconnected pores, paper presented at Fifth International Conference on Gas Hydrates, Trondheim, Norway, 13–16 June.

Bachrach, R., J. Dvorkin, and A. M. Nur (2000), Seismic velocities and Poisson's ratio of shallow unconsolidated sands, *Geophysics*, *65*(2), 559–564, doi:10.1190/1.1444751.

Buffett, B. A., and O. Y. Zatespina (2000), Formation of gas hydrate from dissolved gas in natural porous media, *Mar. Geol.*, *164*, 69–77, doi:10.1016/S0025-3227(99)00127-9.

Carmichael, R. S. (1982), *Practical Handbook of Physical Properties of Rocks*, vol. 2, CRC Press, Boca Raton, Fla.

Cascante, G., C. Santamarina, and N. Yassir (1998), Flexural excitation in a standard torsional-resonant column, *Can. Geotech. J.*, *35*, 478–490, doi:10.1139/cgj-35-3-478.

Castagna, J. P., M. L. Batzle, and R. L. Eastwood (1985), Relationships between compressional-wave and shear-wave velocities in clastic silicate rocks, *Geophysics*, *50*(4), 571–581, doi:10.1190/1.1441933.

Chand, S., T. A. Minshull, D. Gei, and J. M. Carcione (2004), Elastic velocity models for gas-hydrate-bearing sediments—A comparison, *Geophys. J. Int.*, *159*(2), 573–579, doi:10.1111/j.1365-246X.2004.02387.x.

Chand, S., T. A. Minshull, J. A. Priest, A. I. Best, C. R. I. Clayton, and W. F. Waite (2006), An effective medium inversion algorithm for gas hydrate quantification and its application to laboratory and borehole measurements of gas hydrate-bearing sediments, *Geophys. J. Int.*, *166*(2), 543–552, doi:10.1111/j.1365-246X.2006.03038.x.

Chang, T., A. Misra, and S. S. Sundaram (1990), Micromechnical modelling of cemented sands under low amplitude oscillations, *Geotechnique*, *40*(2), 251–263.

Chapoy, A., A. H. Mohammadi, D. Richon, and B. Tohidi (2004), Gas solubility measurement and modeling for methane-water and methane-ethane-*n*-butane-water systems at low temperature conditions, *Fluid Phase Equilib.*, *220*, 111–119, doi:10.1016/j.fluid.2004.02.010.

Clayton, C. R. I., J. A. Priest, and A. I. Best (2005), The effects of disseminated methane hydrate on the dynamic stiffness and damping of a sand, *Geotechnique*, *55*(6), 423–434, doi:10.1680/geot.2005.55.6.423.

Clayton, C. R. I., J. A. Priest, M. Bui, A. Zervos, and S. G. Kim (2009), The Stokoe resonant column apparatus: Effects of stiffness, mass and

specimen fixity, *Geotechnique*, *59*(5), 429–437, doi:10.1680/geot.2007.00096.

Clennell, M. B., M. Hovland, J. S. Booth, P. Henry, and W. J. Winters (1999), Formation of natural gas hydrates in marine sediments: 1. Conceptual model of gas hydrate growth conditioned by host sediment properties, *J. Geophys. Res.*, *104*(B10), 22,985–23,003, doi:10.1029/1999JB900175.

Collett, T. S., and J. Ladd (2000), Detection of gas hydrates with downhole logs and assessment of gas hydrate concentrations (saturations) and gas volumes on the Blake Ridge with electrical resistivity log data, *Proc. Ocean Drill. Program, Sci. Results*, *164*, 179–191.

Collett, T. S., M. W. Lee, S. R. Dalimore, and W. F. Agena (1999), Seismic and well-log-inferred gas hydrate accumulations on Richards Island, in *Scientific Results From JAPEX/JNOC/GSC Mallik 2L–38 Gas Hydrate Research Well, Mackenzie Delta, Northwest Territories, Canada*, edited by S. R. Dallimore, T. Uchida, and T. S. Collett, *Bull. Geol. Surv. Can*, *544*, 357–376.

Cresswell, A., M. E. Barton, and M. R. Brown (1999), Determining the maximum dry density of sands by pluviation, *Geotech. Test. J.*, *22*(4), 324–328, doi:10.1520/GTJ11245J.

Dillon, W. P., M. W. Lee, and D. F. Coleman (1994), Identification of marine hydrates in situ and their distribution off the Atlantic coast of the United States, in *Natural Gas Hydrates*, edited by E. D. Sloan, J. Happel, and M. A. Hnatow, *Ann. N. Y. Acad. Sci.*, *715*, 362–380.

Domenico, S. N. (1977), Elastic properties of unconsolidated porous sand reservoirs, *Geophysics*, *42*(7), 1339–1368, doi:10.1190/1.1440797.

Drnevich, V. P., B. O. Hardin, and D. J. Shippy (1978), Modulus and damping of soils by the resonant-column method, in *Dynamic Geotechnical Testing*, *ASTM Spec. Tech. Publ.*, *654*, 91–121.

Duffaut, K., and M. Landrø (2007), V_p/V_s ratio versus differential stress and rock consolidation: A comparison between rock models and time-lapse AVO data, *Geophysics*, *72*(5), C81–C94, doi:10.1190/1.2752175.

Dvorkin, J., and A. Nur (1993), Rock physics for the characterization of gas hydrates, in *The Future of Energy Gases*, edited by D. G. Howell, *U.S. Geol. Surv. Prof. Pap.*, *1570*, 293–298.

Dvorkin, J., and A. Nur (1996), Elasticity of high-porosity sandstones: Theory for two North Sea data sets, *Geophysics*, *61*(5), 1363–1370, doi:10.1190/1.1444059.

Ebinuma, T., Y. Kamata, H. Minagawa, R. Ohmura, J. Nagao, and H. Narita (2005), Mechanical properties of sandy sediments containing methane hydrate, paper presented at Fifth International Conference on Gas Hydrates, Trondheim, Norway, 13–16 June.

Ecker, C., J. Dvorkin, and A. M. Nur (2000), Estimating the amount of gas hydrate and free gas from marine seismic data, *Geophysics*, *65*(2), 565–573, doi:10.1190/1.1444752.

Expedition 311 Scientists (2005), Cascadia Margin gas hydrates, *IODP Prelim. Rep.*, *311*, doi:10.2204/iodp.pr.311.2005.

Gassmann, F. (1951), Über die elastizität poröser medien, *Vierteljahrsschr. Naturforsch. Ges. Zuerich*, *96*, 1–21.

Hamilton, E. L. (1971), Elastic properties of marine sediments, *J. Geophys. Res.*, *76*(2), 579–604, doi:10.1029/JB076i002p00579.

Hamilton, E. L. (1979), V_p/V_s and Poisson's ratios in marine sediments and rocks, *J. Acoust. Soc. Am.*, *66*(4), 1093–1101, doi:10.1121/1.383344.

Handa, Y. P. (1990), Effect of hydrostatic pressure and salinity on the stability of gas hydrates, *J. Phys. Chem.*, *94*, 2652–2657, doi:10.1021/j100369a077.

Haq, B. (1998), Natural gas hydrates: Searching for the long-term climatic and slope stability records, in *Gas Hydrates: Relevance to World Margin Stability and Climate Change*, edited by J.-P. Henriet and J. Meinert, *Geol. Soc. Spec. Publ.*, *137*, 303–318.

Hardin, B. O., and W. L. Black (1968), Vibration modulus of normally consolidated clays, *J. Soil Mech. Found. Div. Am. Soc. Civ. Eng.*, *94*(SM2), 353–369.

Hardin, B. O., and V. P. Drnevich (1972), Shear modulus and damping in soils: Measurement and parameter effects, *J. Soil Mech. Found. Div. Am. Soc. Civ. Eng.*, *98*(7), 603–624.

Helgerud, M. B., J. Dvorkin, A. Nur, A. Sakai, and T. Collett (1999), Elastic-wave velocity in marine sediments with gas hydrates: Effective medium modeling, *Geophys. Res. Lett.*, *26*, 2021–2024, doi:10.1029/1999GL900421.

Huo, Z., K. Hester, E. D. Sloan Jr., and K. T. Miller (2003), Methane hydrate nonstoichiometry and phase diagram, *AIChE J.*, *49*(5), 1300–1306, doi:10.1002/aic.690490521.

Hyndman, R. D., and G. D. Spence (1992), A seismic study of methane hydrate marine bottom simulating reflectors, *J. Geophys. Res.*, *97*(B5), 6683–6698, doi:10.1029/92JB00234.

Kerr, R. A. (2004), Gas hydrate resource: Smaller but sooner, *Science*, *303*, 946–947, doi:10.1126/science.303.5660.946.

Korenaga, J., W. S. Holbrook, S. C. Singh, and T. A. Minshull (1997), Natural gas hydrates on the southeast U.S. margin: Constraints from full waveform and travel time inversions of wide-angle seismic data, *J. Geophys. Res.*, *102*(B7), 15,345–15,365, doi:10.1029/97JB00725.

Kunerth, D. C., D. M. Weinberg, J. W. Rector, C. L. Scott, and J. T. Johnson (2001), Acoustic laboratory measurement during the formation of a THF-hydrate in unconsolidated porous media, *J. Seismic Explor.*, *9*, 337–354.

Kvenvolden, K. A. (1993), Gas hydrates: Geological perspective and global change, *Rev. Geophys.*, *31*, 173–187, doi:10.1029/93RG00268.

Kvenvolden, K. A., and L. A. Barnard (1983), Gas hydrates of the Blake Outer Ridge, Site 533, Deep Sea Drilling Project Leg 76, *Initial Rep. Deep Sea Drill. Proj.*, *76*, 353–365.

Kvenvolden, K. A., and T. D. Lorenson (2001), A global inventory of natural gas hydrate occurrence, in *Natural Gas Hydrates: Occurrence, Distribution, and Detection*, *Geophys. Monogr. Ser*, vol. 124, edited by C. K. Paull and W. P. Dillon, pp. 3–18, AGU, Washington, D. C.

Lee, M. W., and T. Collett (2005), Assessment of gas hydrate concentrations estimated from sonic logs in the JAPEX/JNOC/GSC et al. Mallik 5L–38 gas hydrate production well, in *Scientific Results From the Mallik 2002 Gas Hydrate Production Research Well Program, Mackenzie Delta, Northwest Territories, Canada*, edited by S. R. Dallimore and T. S. Collett, *Bull. Geol. Surv. Can*, 585, 10 pp.

Lee, M. W., and W. F. Waite (2008), Estimating pore-space gas hydrate saturations from well log acoustic data, *Geochem. Geophys. Geosyst.*, *9*, Q07008, doi:10.1029/2008GC002081.

Lee, J. Y., T. S. Yun, J. C. Santamarina, and C. Ruppel (2007), Observations related to tetrahydrofuran and methane hydrates for laboratory studies of hydrate-bearing sediments, *Geochem. Geophys. Geosyst.*, *8*, Q06003, doi:10.1029/2006GC001531.

Makse, H. A., N. Gland, D. L. Johnson, and L. Schwartz (2004), Granular packings: Nonlinear elasticity, sound propagation, and collective relaxation dynamics, *Phys. Rev. E*, *70*, 061302, doi:10.1103/PhysRevE.70.061302.

Mavko, G., T. Mukerji, and J. Dvorkin (1998), *The Rock Physics Handbook: Tools for Seismic Analysis in Porous Media*, Cambridge Univ. Press, Cambridge, U. K.

Meinert, J., J. Posewang, and M. Baumann (1998), Gas hydrates along the northeastern Atlantic margin: Possible hydrate-bound margin instabilities and possible release of methane, in *Gas Hydrates: Relevance to World Margin Stability and Climate Change*, edited by J.-P. Henriet and J. Meinert, *Geol. Soc. Spec. Publ.*, *137*, 275–291.

Nixon, M. F., and J. L. H. Grozic (2007), Submarine slope failure due to gas hydrate dissociation: A preliminary quantification, *Can. Geotech. J.*, *44*, 314–325, doi:10.1139/T06-121.

Paull, C. K., et al. (1996), *Proceedings of the Ocean Drilling Program, Initial Reports*, vol. 164, Ocean Drill. Program, College Station, Tex.

Peng, D. Y., and D. B. Robinson (1976), A new two-constant equation of state, *Ind. Eng. Chem. Fundam.*, *15*, 59–64, doi:10.1021/i160057a011.

Prasad, M. (2002), Acoustic measurements in unconsolidated sands at low effective pressure and overpressure detection, *Geophysics*, *67*(2), 405–412, doi:10.1190/1.1468600.

Priest, J. A., A. I. Best, and C. R. I. Clayton (2005), A laboratory investigation into the seismic velocities of methane gas hydrate-bearing sand, *J. Geophys. Res.*, *110*, B04102, doi:10.1029/2004JB003259.

Rad, N. S., and M. T. Tumay (1987), Factors affecting sand specimen preparation by raining, *Geotech. Test. J.*, *10*(1), 31–37, doi:10.1520/GTJ10136J.

Richart, F. E., J. R. Hall, and R. D. Woods (1970), *Vibration of Soils and Foundations*, Prentice-Hall, Englewood Cliffs, N. J.

Ruppel, C. (2007), Tapping methane hydrates for unconventional natural gas, *Elements*, *3*, 193–199, doi:10.2113/gselements.3.3.193.

Santamarina, J. C., K. A. Klein, and M. A. Fam (2001), *Soils and Waves, John Wiley*, Chichester, U. K.

Saxena, S. K., A. S. Avramidis, and K. R. Reddy (1988), Dynamic moduli and damping ratios of cemented sands at low strains, *Can. Geotech. J.*, *25*, 353–368, doi:10.1139/t88-036.

Schultheiss, P. J., et al. (2006), Pressure coring, logging and subsampling with the HYACINTH system, in *New Ways of Looking at Sediment Cores and Core Data*, edited by R. G. Rothwell, *Geol. Soc. Spec. Publ.*, *267*, 151–163.

Schultheiss, P. J., M. Holland, and G. D. Humphrey (2008), Borehole pressure coring and laboratory pressure core analysis for gas hydrate investigations, paper presented at Offshore Technology Conference, Houston, Tex., 5–8 May.

Shillington, D. J., T. A. Minshull, C. Peirce, and J. M. O'Sullivan (2008), P- and S-wave velocities of consolidated sediments from a seafloor seismic survey in the North Celtic Sea Basin, offshore Ireland, *Geophys. Prospect.*, *56*(2), 197–211, doi:10.1111/j.1365-2478.2007.00669.x.

Sloan, E. D., Jr. (1998), *Clathrate Hydrates of Natural Gases*, Marcel Dekker, New York.

Spangenberg, E., J. Kulenkampff, R. Naumann, and J. Erzinger (2005), Pore space hydrate formation from methane dissolved in water, *Geophys. Res. Lett.*, *32*, L24301, doi:10.1029/2005GL024107.

Spangenberg, E., B. Beeskow-Strauch, M. Luzi, R. Naumann, and J. M. Schicks (2008), The process of hydrate formation in clastic sediments and its impact on their physical properties, paper presented at Sixth International Conference on Gas Hydrates, Sponsor, Vancouver, B. C., Canada, 6–10 July.

Stoll, R. D., and G. M. Bryan (1979), Physical properties of sediments containing gas hydrates, *J. Geophys. Res.*, *84*(B4), 1629–1634, doi:10.1029/JB084iB04p01629.

Sultan, N., P. Cochonat, J.-P. Foucher, and J. Mienert (2004), Effect of gas hydrate melting on seafloor slope instability, *Mar. Geol.*, *213*, 379–401, doi:10.1016/j.margeo.2004.10.015.

Tohidi, B., R. Anderson, M. B. Clennell, R. W. Burgass, and A. B. Biderkab (2001), Visual observation of gas-hydrate formation and dissociation in synthetic porous media by means of glass micromodels, *Geology*, *29*(9), 867–870, doi:10.1130/0091-7613(2001)029<0867:VOOGHF>2.0.CO;2.

Tréhu, A. M., et al. (2003), *Proceedings of the Ocean Drilling Program, Initial Reports*, vol. 204, Ocean Drill. Program, College Station, Tex.

Waite, W. F., W. J. Winters, and D. H. Mason (2004), Methane hydrate formation in partially water-saturated Ottawa sand, *Am. Mineral.*, *89*, 1202–1207.

Wilkens, R., G. Simmons, and L. Caruso (1984), The ratio V_p/V_s as a discriminant of composition for siliceous limestones, *Geophysics*, *49*(11), 1850–1860, doi:10.1190/1.1441598.

Winters, W. J., W. P. Dillon, I. A. Pecher, and D. H. Mason (2000), GHASTLI—Determining physical properties of sediment containing natural and laboratory-formed gas hydrates, in *Natural Gas Hydrate in Oceanic and Permafrost Environments*, edited by M. D. Max, pp. 311–322, Kluwer Acad., Norwell, Mass.

Winters, W. J., I. A. Pecher, W. F. Waite, and D. H. Mason (2004), Physical properties and rock physics models of sediment containing natural and laboratory-formed methane gas hydrate, *Am. Mineral.*, *89*, 1221–1227.

Yang, J., B. Tohidi, and A. Chapoy (2008), Impact of sedimentary mineralogy on the geophysical and geomechanical properties of hydrate-bearing sediments, paper presented at Sixth International Conference on Gas Hydrates, Sponsor, Vancouver, B. C., Canada, 6–10 July.

Yun, T. S., F. M. Francisca, J. C. Santamarina, and C. Ruppel (2005), Compressional and shear wave velocities in uncemented sediment containing gas hydrate, *Geophys. Res. Lett.*, *32*, L10609, doi:10.1029/2005GL022607.

Yun, T. S., G. A. Narsilio, J. C. Santamarina, and C. Ruppel (2006), Instrumented pressure chamber for characterizing sediment cores recovered at in situ hydrostatic pressure, *Mar. Geol.*, *229*, 285–293, doi:10.1016/j.margeo.2006.03.012.

Yun, T. S., J. C. Santamarina, and C. Ruppel (2007), Mechanical properties of sand, silt, and clay containing tetrahydrofuran hydrate, *J. Geophys. Res.*, *112*, B04106, doi:10.1029/2006JB004484.

Zhang, W., J. L. Creek, and C. A. Koh (2001), A novel multiple cell photosensor instrument: Principles and application to the study of THF hydrate formation, *Meas. Sci. Technol.*, *12*, 1620–1630, doi:10.1088/0957-0233/12/10/302.

Zimmer, M. A., M. Prasad, G. Mavko, and A. Nur (2007), Seismic velocities of unconsolidated sands: Part 1—Pressure trends from 0.1 to 20 MPa, *Geophysics*, *72*(1), E1–E13, doi:10.1190/1.2399459.

C. R. I. Clayton, J. A. Priest, and E. V. L. Rees, School of Civil Engineering, University of Southampton, Southampton SO17 1BJ, UK. (j.a.priest@soton.ac.uk)